



**HAL**  
open science

## Impulsive zone model predictive control for rendezvous hovering phases

Christophe Louembet, Alejandro Hernan Gonzalez, Paulo Ricardo Arantes Gilz

► **To cite this version:**

Christophe Louembet, Alejandro Hernan Gonzalez, Paulo Ricardo Arantes Gilz. Impulsive zone model predictive control for rendezvous hovering phases. Conference on Decision and Control, Dec 2019, Nice, France. hal-02154952

**HAL Id: hal-02154952**

**<https://laas.hal.science/hal-02154952>**

Submitted on 13 Jun 2019

**HAL** is a multi-disciplinary open access archive for the deposit and dissemination of scientific research documents, whether they are published or not. The documents may come from teaching and research institutions in France or abroad, or from public or private research centers.

L'archive ouverte pluridisciplinaire **HAL**, est destinée au dépôt et à la diffusion de documents scientifiques de niveau recherche, publiés ou non, émanant des établissements d'enseignement et de recherche français ou étrangers, des laboratoires publics ou privés.

# Impulsive zone model predictive control for rendezvous hovering phases

Christophe Louembet<sup>1</sup>, Alejandro H. González<sup>2</sup> and Paulo R. Arantes Gilz<sup>1</sup>

**Abstract**—In this manuscript, an impulsive zone MPC formulation is proposed to tackle the problem of the spacecraft rendezvous control. The control objective is to maintain the follower spacecraft in a given subspace with respect to a leader vehicle by stabilizing the set of periodic relative orbits included in a given hovering zone. The idea is to incorporate this hovering zone as a target set into the MPC cost function, in order to permit a single MPC formulation and a receding horizon implementation. The control algorithm takes advantages of a relative motion parametrization for which the set of the equilibrium states represent the set of periodic orbits to prove the stability of the hovering zone and to enlarge significantly the domain of attraction. Several simulation results show that, in addition, performances in terms of convergence and fuel consumption are improved in comparison with previous works.

**Keywords:** Spacecraft rendezvous, Zone MPC, Impulsive control system

## I. INTRODUCTION

In the context of the industrial development of on-orbit services (see [1]), mastering spacecraft rendezvous is a priority and, from the approaching phases to closing maneuvers, the feedback control algorithm is crucial. This work addresses the hovering phase of a rendezvous mission. This phase – which is useful for measurement tasks, safe observation, synchronization or simply waiting for mission control decision – consists in controlling the position of a deputy spacecraft relatively to a leader vehicle.

The leader spacecraft is assumed to be inert and evolves on its natural orbit while the deputy is able to control its orbit by means of chemical thrusters. Contrary to electrical thrusters, chemical engines provide high thrusts on short periods of time compared to space mechanics time constants (basically the orbital period). Considering a large time scale difference between the relative motion dynamics and the control effects on them, the control signal will be therefore modeled as an impulsive signal. Thus, the addressed problem in this paper can be classified as impulsive control systems (ICS, [2]) from a dynamical systems point of view.

Rendezvous guidance and control under impulsive assumption leads to a venue of works since the beginning of the century (see the review papers [3], [4]). Among different

control frameworks, Model Predictive Control (MPC) has been the most popular one because it ensures stability while minimizing a flexible objective function (the cost) and satisfying technological constraints (thrusters saturation, safe path constraints, etc.). For instance, different safety requirements have been addressed such as visibility constraints [5], collision or plume avoidance [6], [7], or hovering [8]. Thanks to MPC properties, stability can be proved even in presence of obstacle avoidance requirements [9]. Robust performances can also be guaranteed using *constraint tightening MPC* (see [10] and references therein) or *tube-based MPC* (see [11] and references therein). Moreover, it has also been shown that this family of optimization-based algorithms can effectively be onboarded on real spaceflight devices ([12], [13]).

In a more general frame, ICS have received great attention in the last decade, specially in the field of biomedical research (diseases treatments, where the drug intakes are of short duration). To propose a proper MPC formulation in this context, two main problems had to be solved: the characterization of generalized equilibrium and invariant sets of ICS (out of the trivial case of the origin) and the consideration of entire sets (instead of points) as control objective (zone control). The control objective is, in any case, that discontinuous and non stationary state trajectories of ICS remain in the objective set upon convergence. Two different approaches in this line were presented in [14], [15], [16].

In this work, the basic ideas underlying the so-called impulsive zone MPC (IzMPC) of [15] are used to propose a new controller, specifically formulated for the guidance of a rendezvous to a given hovering zone. To this ends, some interesting periodicity properties – coming from the formal description of the periodic relative orbits included in a given polytope (developed in several recent works, [17], [18], [19]) – are exploited. The benefits of these properties in the context of IzMPC can be described three fold: it ensures recursive feasibility and closed-loop stability, it has an enlarged domain of attraction (in a rather natural form, without using additional optimization variables) and it shows a good performance (in terms of the objective function, convergence rate and fuel consumption) in comparison with other recent strategies [20], [19].

The organization of the paper is as follows. In Section II, the modeling details of the hovering zone problem are presented, including some useful similarity transformations, a description of the impulsive nature of the controls and the characterization of the hovering constraint zone. Then, in Section III, the proposed IzMPC controller is presented, while the stability of the resulting closed-loop is proved in Section IV. In Section V, a comparison of the controller

<sup>1</sup>LAAS-CNRS, Université de Toulouse, CNRS, 7 Avenue du Colonel Roche, F-31031, Toulouse, France. louembet@laas.fr

<sup>2</sup>Institute of Technological Development for the Chemical Industry (INTEC), CONICET-Universidad Nacional del Litoral (UNL). Güemes 3450, (3000) Santa Fe, Argentina alejgon@santafe-conicet.gov.ar

performance with other existing strategies is performed, by means of some numerical simulations. Finally, in Section VI, the conclusions of the work are given.

## II. MODELING THE HOVERING PROBLEM

In this section, the relative dynamics will be first exposed in terms of cartesian state  $X$ . Then, the Deaconu parametrization of the relative motion is introduced as a specific state with its own dynamics and closed-form transition. In a second step, the hovering zone problem is described in terms of constraints on the relative state: the admissible set of relative orbits is defined by means of linear matrix inequalities. This definition will be then used in the development of the predictive control law.

### A. Relative dynamics and motion parametrization

The relative motion consists in the motion of a follower spacecraft  $S_f$  with respect to a passive target spacecraft  $S_l$ . It is modeled in the frame centered on the leader spacecraft, namely Local Vertical / Local Horizontal (LVLH) frame, given by  $\{S_l, \vec{x}, \vec{y}, \vec{z}\}$ , rotating with respect to the Earth-Centered Inertial (ECI) frame, given by  $\{O, \vec{I}, \vec{J}, \vec{K}\}$  (see [21] for details). Under Keplerian assumptions, the leader orbit is located by the true anomaly  $\nu$  on its orbit, mainly described by its semi-major axis  $a$  and its eccentricity  $0 < e < 1$ .

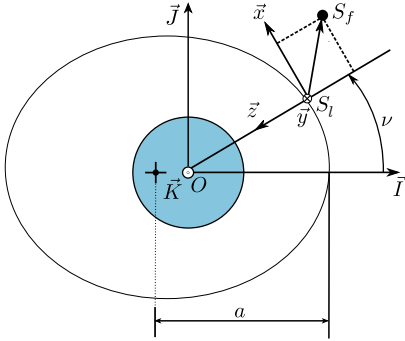


Fig. 1: Inertial and relative frames.

The relative motion  $\overrightarrow{S_l S_f}$  is defined as the time history of the relative vector  $\overrightarrow{S_l S_f}$  in figure 1. Its state representation is given by the relative position and velocity,  $X(t) = [x(t), y(t), z(t), \dot{x}(t), \dot{y}(t), \dot{z}(t)]^T$ . Assuming the relative navigation hypothesis i.e.  $\|S_l S_f\| \ll \|O S_l\|$ , linearized state dynamic equation is provided in [22]:

$$\dot{X}(t) = \underbrace{\begin{bmatrix} 0 & 0 & 0 & 1 & 0 & 0 \\ 0 & 0 & 0 & 0 & 1 & 0 \\ 0 & 0 & 0 & 0 & 0 & 1 \\ \dot{\nu}^2 - \frac{\mu}{R^3} & 0 & \ddot{\nu} & 0 & 0 & 2\dot{\nu} \\ 0 & -\frac{\mu}{R^3} & 0 & 0 & 0 & 0 \\ \ddot{\nu} & 0 & \dot{\nu}^2 + 2\frac{\mu}{R^3} & -2\dot{\nu} & 0 & 0 \end{bmatrix}}_{A(t)} X(t), \quad (1)$$

where the time varying dynamic matrix depends on the true anomaly,  $\nu$ , and the orbital parameters of the leader  $\dot{\nu} = \sqrt{\frac{\mu}{a^3(1-e^2)^3}}(1+e \cos \nu)^2$ , being  $\mu$  the Earth's gravitational

constant,  $a$  the semi-major axis, and  $0 < e < 1$  the leader orbit eccentricity.

A simplified version of (1) is obtained by replacing the time  $t$  by the true anomaly  $\nu$  as independent variable and applying the following similarity transformation

$$\tilde{X}(\nu) = \underbrace{\begin{bmatrix} (1+ec_\nu)\mathbb{I}_3 & \mathbb{O}_3 \\ -es_\nu\mathbb{I}_3 & \sqrt{\frac{a^3(1-e^2)^3}{\mu(1+ec_\nu)^2}}\mathbb{I}_3 \end{bmatrix}}_{T(\nu)} X(t), \quad (2)$$

where the notation  $c_\nu = \cos \nu$  and  $s_\nu = \sin \nu$  are employed. Thus, the true-anomaly-dependent state  $\tilde{X}(\nu) = [\tilde{x}(\nu), \tilde{y}(\nu), \tilde{z}(\nu), \tilde{x}'(\nu), \tilde{y}'(\nu), \tilde{z}'(\nu)]^T$  is defined along with its simplified dynamics [23]:

$$\tilde{X}'(\nu) = \underbrace{\begin{bmatrix} 0 & 0 & 0 & 1 & 0 & 0 \\ 0 & 0 & 0 & 0 & 1 & 0 \\ 0 & 0 & 0 & 0 & 0 & 1 \\ 0 & 0 & 0 & 0 & 0 & 2 \\ 0 & 0 & 0 & 0 & -1 & 0 \\ 0 & 0 & \frac{3}{\rho_\nu} & -2 & 0 & 0 \end{bmatrix}}_{\tilde{A}(\nu)} \tilde{X}(\nu), \quad (3)$$

where  $\rho_\nu = 1 + e \cos \nu$ . The main advantage of this state representation is that a closed-form solution exists ([23]) such that:

$$\tilde{X}(\nu) = \Psi(\nu, \nu_0) \tilde{X}(\nu_0) = \psi(\nu) \psi^{-1}(\nu_0) \tilde{X}(\nu_0), \quad (4)$$

where  $\psi(\nu)$  is the fundamental matrix. In [17], a parametrization of the relative trajectories (4) is proposed such that:

$$D(\nu) = \underbrace{\begin{bmatrix} 0 & -(3ec_\nu + e^2 + 2) & \rho_\nu^2 & -es_\nu \rho_\nu & 0 & 0 \\ 0 & 3(e + c_\nu) & -(2c_\nu + ec_\nu^2 + e) & s_\nu \rho_\nu & 0 & 0 \\ 0 & \frac{3s_\nu(\rho_\nu + e^2)}{\rho_\nu} & -s_\nu(2 + ec_\nu) & 2e - c_\nu \rho_\nu & 0 & 0 \\ 1 & \frac{3es_\nu(2 + ec_\nu)}{\rho_\nu} & es_\nu(2 + ec_\nu) & ec_\nu \rho_\nu - 2 & 0 & 0 \\ 0 & 0 & 0 & 0 & c_\nu & -s_\nu \\ 0 & 0 & 0 & 0 & s_\nu & c_\nu \end{bmatrix}}_{C(\nu)} \tilde{X}(\nu). \quad (5)$$

$D(\nu) = [d_0(\nu), d_1(\nu), d_2(\nu), d_3(\nu), d_4(\nu), d_5(\nu)]^T$  is the so-called vector of Deaconu parameters (see [11] [17]). Since matrix  $C(\nu)$  is invertible, (5) defines a similarity transformation and  $D$  is a proper state vector for the relative motion. Its dynamics is given by

$$D'(\nu) = \underbrace{\begin{bmatrix} 0 & 0 & 0 & 0 & 0 & 0 \\ 0 & 0 & 0 & 0 & 0 & 0 \\ -\frac{3e}{\rho(\nu)^2} & 0 & 0 & 0 & 0 & 0 \\ \frac{3}{\rho(\nu)^2} & 0 & 0 & 0 & 0 & 0 \\ 0 & 0 & 0 & 0 & 0 & 0 \\ 0 & 0 & 0 & 0 & 0 & 0 \end{bmatrix}}_{A_D(\nu)} D(\nu). \quad (6)$$

A closed-form solution to the differential equation (6) exists, and it is given by:

$$D(\nu) = \underbrace{\begin{bmatrix} 1 & 0 & 0 & 0 & 0 & 0 \\ 0 & 1 & 0 & 0 & 0 & 0 \\ -3eJ_{\nu_0}(\nu) & 0 & 1 & 0 & 0 & 0 \\ 3J_{\nu_0}(\nu) & 0 & 0 & 1 & 0 & 0 \\ 0 & 0 & 0 & 0 & 1 & 0 \\ 0 & 0 & 0 & 0 & 0 & 1 \end{bmatrix}}_{\Phi(\nu, \nu_0)} D(\nu_0), \quad (7)$$

where

$$J_{\nu_0}(\nu) := \int_{\nu_0}^{\nu} \frac{d\tau}{(1+e \cos \tau)^2} = \sqrt{\frac{\mu}{a^3}} \frac{t-t_0}{(1-e^2)^{3/2}}. \quad (8)$$

This parametrization of the relative motion provides a direct insight on the geometry of the relative orbits like the relative orbital elements exploited in [24]. For instance, the Cartesian relative position are expressed linearly in terms of  $D$  states as:

$$\begin{aligned}\tilde{x}(\nu) &= d_1(1 + \rho)s_\nu - d_2(1 + \rho)c_\nu + d_3 + 3d_0J(\nu)\rho^2, \\ \tilde{y}(\nu) &= d_4c_\nu + d_5s_\nu, \\ \tilde{z}(\nu) &= d_1\rho c_\nu + d_2\rho s_\nu - 3ed_0J(\nu)s_\nu\rho + 2d_0,\end{aligned}\quad (9)$$

On one hand, one can notice in (6) that  $D'(\nu) = 0$  whenever  $d_0(\nu) = 0$ . Thus, the condition  $d_0(\nu) = 0$  defines the equilibrium states for the representation  $D$ . On the other hand, the condition  $d_0 = 0$  implies that the position transition is periodic according to (9). Thereby, the set of equilibrium points of (6) is equivalent to the set of the relative periodic orbits in the Cartesian coordinates and will therefore be denoted

$$\mathcal{D}_s = \{D \in \mathbb{R}^6 : d_0 = 0\}.\quad (10)$$

### B. Impulsive Control System

The chaser vehicle is assumed to have 6 thrusters aligned by pairs along each axis of the rotating frame so that each axis are fully controlled. Moreover, the control signal is considered as impulsive by the virtue of the chemical propulsion assumption. The control instants  $\nu_k$  are separated by a constant  $\Delta\nu$  time. The impulsive control at a given time  $\nu_k$ , with  $k \in \mathbb{N}$ , is denoted

$$\Delta V(\nu_k) = [\Delta V_x(\nu_k), \Delta V_y(\nu_k), \Delta V_z(\nu_k)]^T \in \mathbb{R}^3.\quad (11)$$

The impulsive control system (ICS) is now defined by

$$\begin{cases} D'(\nu) &= A_D(\nu)D(\nu), \quad D(0) = D_0, \quad \nu \neq \nu_k, \\ D(\nu_k^+) &= D(\nu_k) + B_D(\nu_k)\Delta V(\nu_k), \quad k \in \mathbb{N}, \end{cases}\quad (12)$$

where  $B_D(\nu) = C(\nu)T(\nu)B$  with  $B = [0_3 \ \mathbb{I}_3]^T$ . Following the ideas presented in [15], it is possible to associate two discrete-time systems to the latter impulsive system. The first one, which describes the system just before the impulsive controls are injected, is given by:

$$D(\nu_{k+1}) = \Phi(\nu_{k+1}, \nu_k)D(\nu_k) + \Phi(\nu_{k+1}, \nu_k)B_D(\nu_k)\Delta V(\nu_k).\quad (13)$$

The second system, which describes the system evolution just after the impulses, is given by:

$$D(\nu_{k+1}^+) = \Phi(\nu_{k+1}, \nu_k)D(\nu_k^+) + B_D(\nu_{k+1})\Delta V(\nu_{k+1}),\quad (14)$$

where  $D(\nu_k^+) = D(\nu_k) + B_D(\nu_k)\Delta V(\nu_k)$ . In the addressed control problem, control input saturation will be accounted for. Therefore, each thruster is limited in thrust magnitude so that the input constraints are described by

$$\|\Delta V(\nu_k)\|_\infty \leq \overline{\Delta V}, \quad \forall \nu_k.\quad (15)$$

For sake of simplicity, the following notations are adopted

$$\begin{aligned}D_k &= D(\nu_k), \\ D_k^+ &= D^+(\nu_k), \\ \Phi_k &= \Phi(\nu_{k+1}, \nu_k), \\ B_k &= \Phi(\nu_{k+1}, \nu_k)B_D(\nu_k).\end{aligned}\quad (16)$$

where  $\Phi(\nu_{k+1}, \nu_k)$  is the transition matrix between time  $\nu_k$  and  $\nu_{k+1}$  (as defined in equation (7)). In the sequel, we will consider that the control time instants,  $\{\nu_k\}$ , are equidistant so that  $\nu_{k+1} - \nu_k = \Delta\nu$ , for all  $k \in \mathbb{N}$ .

### C. Hovering constraints

The aim of the control problem is to reach and stabilize the hovering zone in the relative state space accounting for the control input saturation (15).

During the hovering phases, the follower is required to remain inside of a given limited region. This hovering zone is described without loss of generality by a cuboid in terms of Cartesian relative position:

$$\underline{x} \leq x(t) \leq \bar{x}, \quad \underline{y} \leq y(t) \leq \bar{y}, \quad \underline{z} \leq z(t) \leq \bar{z}, \quad \forall t \geq t_0.\quad (17)$$

By applying the changes of variables (5) and (2), the set of inequalities (17) can be rewritten in terms of  $D$  state:

$$\underline{x} \leq M_x(\nu)D \leq \bar{x}, \quad \underline{y} \leq M_y(\nu)D \leq \bar{y}, \quad \underline{z} \leq M_z(\nu)D \leq \bar{z}, \quad \forall \nu,\quad (18)$$

where

$$\begin{aligned}M_x(\nu) &= \left[ 3eJ_{\nu_0}(\nu)(1 + e c_\nu), \quad \frac{(2+e c_\nu)s_\nu}{1+e c_\nu}, \quad \frac{-(2+e c_\nu)c_\nu}{1+e c_\nu}, \quad \frac{1}{1+e c_\nu}, \quad 0, \quad 0 \right] \\ M_y(\nu) &= \left[ 0, \quad 0, \quad 0, \quad 0, \quad \frac{c_\nu}{1+e c_\nu}, \quad \frac{s_\nu}{1+e c_\nu} \right] \\ M_z(\nu) &= \left[ -3eJ_{\nu_0}(\nu)s_\nu + \frac{2}{1+e c_\nu}, \quad c_\nu, \quad s_\nu, \quad 0, \quad 0, \quad 0 \right]\end{aligned}\quad (19)$$

Contrary to previously published papers (see [8], [25]), the hovering approach is based on periodic relative orbits. According to [26], the periodicity property is interesting from fuel-consumption point of view. In fact, when these periodic orbits are reached, the follower spacecraft is ensured to have a bounded free motion in the absence of exogenous disturbances. Moreover, if the position constraints (17) are satisfied by the periodic orbit tracked by the follower spacecraft, no further corrective control are required to ensure the hovering conditions.

In [18], the set of periodic orbits that belongs to the tolerance cuboid has been defined as

$$S_D = \{D \in \mathbb{R}^6 : D \in \mathcal{D}_s, \text{ and } (18).\}\quad (20)$$

Since inequalities from (18) must be satisfied for all values of  $\nu$ ,  $S_D$  is described by infinitely many constraints. To obtain a finite description of  $S_D$ , [17] exploits results on non-negative polynomials from [27] to boil down the inequalities (18) into LMI conditions:

$$\gamma_l(D) = \Lambda^*(Y_l), \quad Y_l \succeq 0, \quad l = \{\underline{x}, \bar{x}, \underline{y}, \bar{y}, \underline{z}, \bar{z}\},\quad (21)$$

where  $\gamma_l(\cdot)$  are a linear combination of state  $D$  (see [17] for more details). Finally the set of constrained periodic orbits

can be finitely described as

$$S_D = \{D \in \mathbb{R}^6 : d_0 = 0, \gamma_l(D) = \Lambda^*(Y_l), Y_l \succeq 0, \dots, l = \{\underline{x}, \bar{x}, \underline{y}, \bar{y}, \underline{z}, \bar{z}\}\} \quad (22)$$

An alternative description of  $S_D$  can be found in [18] where it is described in terms semi-algebraic set:

$$S_D = \{D \in \mathbb{R}^6 : g_l(D), \leq 0, l = \{\underline{x}, \bar{x}, \underline{y}, \bar{y}, \underline{z}, \bar{z}\}, \quad (23)$$

where  $g_l(\cdot)$  are multivariate polynomials in  $D$ . In any case, it should be noted that  $S_D$  is proved to be compact and convex [19].

### III. MPC FORMULATION

The control objective is to reach the hovering zone,  $S_D$ , by controlling the discrete-time system (13).

The proposed cost function is given by

$$J_N(D_k, S_D; \mathbf{u}_k) \triangleq \sum_{j=0}^{N-1} \alpha \text{dist}_{S_D}(D_{k+j|k}) + \dots \beta \|\Delta V_{k+j|k}\|_l + \gamma \text{dist}_{S_D}(D_{k+N|k}) \quad (24)$$

where  $D_{k|k} = D_k = D(\nu_k)$  is the current state,  $D_{k+j|k}$  denotes the state at time  $\nu_{k+j}$ , predicted at time  $\nu_k$ ,  $\mathbf{u} = \{\Delta V_{k|k}, \Delta V_{k+1|k}, \dots, \Delta V_{k+N-1|k}\}$  is the future input sequence, predicted at time  $\nu_k$ , and  $\text{dist}_{S_D}(D)$  denotes the distance from state  $D$  to set  $S_D$ . Furthermore,  $\|\cdot\|_l$  denotes a norm of order  $l$ , while  $\alpha$ ,  $\beta$  and  $\gamma$  are positive penalization scalars.  $l \in \mathbb{N}$  is to be set to precise whether the consumption ( $l = 1$ ) or the control energy ( $l = 2$ ) is considered.

For sake of clarity, the order of the norm function are omitted since they are straightforward (the distance to  $S_D$  is evaluated through a 2-norm and  $l$ -norm is applied to control variables,  $l = \{1, 2\}$ ).

*Remark 1:* The distance function is defined as  $\text{dist}_{S_D}(D) = \min_{D^* \in S_D} \|D - D^*\|$ . So, the terms  $\text{dist}_{S_D}(D_{k+j|k})$ ,  $j \in \mathbb{I}_{0:N}$ , in cost 24, could be replaced by  $\|D_{k+j|k} - D_{k+j|k}^*\|_l$ , with  $l \in \mathbb{N}$ , and an additional constraint of the form  $D_{k+j|k}^* \in S_D$ , for  $j \in \mathbb{I}_{0:N}$ . This way,  $N$  new optimization variables need to be considered.

The MPC Optimization Problem, solved at each time  $\nu_k$ ,  $k \in \mathbb{N}$ , can be written as:

$$P_{MPC}(D_k) : \min_{\mathbf{u}_k} J_N(D_k, S_D; \mathbf{u}_k) \quad \text{s.t.} \quad \begin{cases} D_{k|k} = D_k, \\ D_{k+j+1|k} = \Phi_{k+j} D_{k+j|k} + B_{k+j} \Delta V_{k+j|k}, \\ \|\Delta V_{k+j|k}\|_\infty \leq \bar{\Delta V}, \quad j \in \mathbb{I}_{0:N-1}, \\ D_{k+N|k} \in \mathcal{D}_s, \end{cases}$$

In the later problem,  $D_k$  (the current state at time  $\nu_k$ ) and  $S_D$  are the optimization parameters, while  $\mathbf{u}_k$  is the optimization variable. The first two constraints account for the system dynamic (13), at each step of the prediction (recalling that  $\Phi(\nu_{k+j+1}, \nu_{k+j})$  is denoted as  $\Phi_{k+j}$  and  $\Phi(\nu_{k+j+1}, \nu_{k+j}) B_D(\nu_{k+j})$  as  $B_{k+j}$ , for simplicity). The third one is the input constraint. The fourth constraint is the stability constraint forcing the state at the end of the

prediction horizon to be in a terminal set given by  $\mathcal{D}_s$  (the equilibrium set), which clearly contains  $S_D$ .

Once problem  $P_{MPC}$  is solved at time  $\nu_k$ , the optimal solution is given by the optimal input sequence

$$\mathbf{u}_k^0 = \{\Delta V_{k|k}^0, \Delta V_{k+1|k}^0, \dots, \Delta V_{k+N-1|k}^0\}, \quad (25)$$

while the optimal cost is denoted as  $J_N^0(D_k, S_D) \triangleq J_N(D_k, S_D; \mathbf{u}_k^0)$ . The control law, derived from the application of a receding horizon control policy (RHC), is given by  $\Delta V_k = \kappa_{MPC}(D_k) = \Delta V_{k|k}^0$ , where  $\Delta V_{k|k}^0$  is the first element of the solution sequence  $\mathbf{u}_k^0$ .

### IV. ASYMPTOTIC STABILITY OF $S_D$

The following theorem summarizes the stability properties of the proposed MPC formulation.

*Theorem 1:* Let us consider the MPC derived from the solution to Problem  $P_{MPC}(D_k)$ . Then, target set  $S_D$  is asymptotically stable for the closed-loop system  $D_{k+1} = \Phi_k D_k + B_k \kappa_{MPC}(D_k)$ , with a domain of attraction given by the controllable set in  $N$  steps to the terminal set  $\mathcal{D}_s$ ,  $\mathcal{C}_N(\mathcal{D}_s)$ .

*Proof:* As usual in the context of MPC, asymptotic stability of the objective set  $S_D$  will be shown in three steps: recursive feasibility, attractivity and stability.

#### *Recursive feasibility of $P_{MPC}$*

Let us consider a state  $D_k \in \mathcal{C}_N(\mathcal{D}_s)$ , and the optimal solution to  $P_{MPC}(D_k)$ ,  $\mathbf{u}_k^0$ , for the current time  $\nu_k$ . The corresponding optimal state sequence is given by  $\mathbf{D}_k^0 = \{D_{k|k}^0, D_{k+1|k}^0, \dots, D_{k+N-1|k}^0, D_{k+N|k}^0\}$ . The optimal cost function, associated to  $\mathbf{u}_k^0$ , is given by  $J_N^0(D_k, S_D) \triangleq J_N(D_k, S_D; \mathbf{u}_k^0)$ .

Now, once the MPC control law  $\Delta V_k = \kappa_{MPC}(D_k) = \Delta V_{k|k}^0$  is applied to the system, the state  $D_{k+1}$  is given by

$$D_{k+1} = \Phi_k D_k + B_k \Delta V_k = \Phi_k D_k + B_k \Delta V_{k|k}^0 = D_{k+1|k}^0, \quad (26)$$

which means that the state  $D_{k+1}$  coincides with the the optimal predicted state  $D_{k+1|k}^0$  (undisturbed case).

Consider the following feasible solution candidates for problem  $P_{MPC}(D_{k+1})$  (i.e. the optimization problem at time  $\nu_{k+1}$ ):

$$\tilde{\mathbf{u}} = \{\Delta V_{k+1|k}^0, \Delta V_{k+2|k}^0, \dots, \Delta V_{k+N-1|k}^0, \tilde{\Delta V}\}, \quad (27)$$

where  $\Delta V_{k+i|k}^0$ ,  $i \in \mathbb{I}_{1:N-1}$ , are the optimal solution of problem  $P_{MPC}(D_k)$  and  $\tilde{\Delta V}$  is a new input that needs to be determined. Clearly,  $\Delta V_{k+i|k}^0$  are feasible for all  $i \in \mathbb{I}_{1:N-1}$ , because of its optimality. The state sequence corresponding to  $\tilde{\mathbf{u}}$  is given by

$$\tilde{\mathbf{D}} = \{D_{k+1|k}^0, D_{k+2|k}^0, \dots, D_{k+N|k}^0, \tilde{D}\}, \quad (28)$$

where  $D_{k+N|k}^0 \in \mathcal{D}_s$  because of the terminal constraint. State  $\tilde{D}$  is given by  $\tilde{D} = \Phi_{k+N} D_{k+N|k}^0 + B_{k+N} \tilde{\Delta V}$ . But, by the invariant condition of  $\mathcal{D}_s$  (Property 1, in the

Appendix), it there exists a feasible input  $\tilde{\Delta V}$  such that  $\tilde{D} \in \mathcal{D}_s$ . Therefore,  $\tilde{\mathbf{u}}$  is a feasible solution to problem  $P_{MPC}(D_{k+1})$ , and so  $P_{MPC}(\cdot)$  is recursively feasible.

#### A. Attractivity of $S_D$

Let us consider the optimal cost of problem  $P_{MPC}(D_k)$ ,  $J_N^0(D_k)$ , for a given state  $D_k \in \mathcal{C}_N(\mathcal{D}_s)$ ,

$$\begin{aligned} J_N^0(D_k) &= J_N(D_k, S_D; \mathbf{u}_k^0) \\ &= \sum_{j=0}^{N-1} \alpha \text{dist}_{S_D}(D_{k+j|k}^0) + \beta \|\Delta V_{k+j|k}^0\| + \gamma \text{dist}_{S_D}(D_{k+N|k}^0). \end{aligned} \quad (29)$$

Consider also the cost obtained for problem  $P_{MPC}(D_{k+1})$  corresponding to the feasible solution of the latter subsection,  $\tilde{\mathbf{u}}$ , denoted as the feasible cost,

$$\begin{aligned} \tilde{J}_N(D_{k+1}) &= J_N(D_{k+1}, S_D; \tilde{\mathbf{u}}) \\ &= \sum_{j=1}^{N-1} \alpha \text{dist}_{S_D}(D_{k+j|k}^0) + \beta \|\Delta V_{k+j|k}^0\| \\ &\quad + \alpha \text{dist}_{S_D}(D_{k+N|k}^0) + \beta \|\tilde{\Delta V}\| + \gamma \text{dist}_{S_D}(\tilde{D}). \end{aligned} \quad (30)$$

The difference between  $\tilde{J}_N(D_{k+1})$  and  $J_N^0(D_k)$  is then given by

$$\begin{aligned} \tilde{J}_N(D_{k+1}) &= J_N^0(D_k) - \alpha \text{dist}_{S_D}(D_{k|k}^0) \\ &\quad - \beta \|\Delta V_{k|k}^0\| - \gamma \text{dist}_{S_D}(D_{k+N|k}^0) \\ &\quad + \beta \|\tilde{\Delta V}\| + \alpha \text{dist}_{S_D}(D_{k+N|k}^0) + \gamma \text{dist}_{S_D}(\tilde{D}), \end{aligned} \quad (31)$$

where  $\tilde{D}$  is the successor state of  $D_{k+N|k}^0$ , when  $\tilde{\Delta V}$  is applied to the system (recall that  $\tilde{D} = \Phi_{k+N} D_{k+N|k}^0 + B_{k+N} \tilde{\Delta V}$ ). From Property 1, in the Appendix, the feasible input  $\tilde{\Delta V}$  of the previous section is such that  $\gamma \text{dist}_{S_D}(\tilde{D}) + (\alpha \text{dist}_{S_D}(D_{k+N|k}^0) + \beta \|\Delta V_{k+N|k}^0\|) \leq \gamma \text{dist}_{S_D}(D_{k+N|k}^0)$ , which means that

$$\tilde{J}_N(D_{k+1}) \leq J_N^0(D_k) - \alpha \text{dist}_{S_D}(D_{k|k}^0) - \beta \|\Delta V_{k|k}^0\|. \quad (32)$$

Now, the optimal cost at time  $k+1$ ,  $J_N^0(D_{k+1})$ , will be (by mere optimality) equal or smaller than any feasible cost. Then  $J_N^0(D_{k+1}) \leq \tilde{J}_N(D_{k+1})$ , and so, from (32) it follows that

$$J_N^0(D_{k+1}) \leq J_N^0(D_k) - \alpha \text{dist}_{S_D}(D_{k|k}^0) - \beta \|\Delta V_{k|k}^0\|. \quad (33)$$

This means that the sequence of costs  $J_N^0(D_k)$  is a decreasing positive real sequence in  $k$ , which converges to a positive value, for  $k \rightarrow \infty$ . This convergence implies that

$$\lim_{k \rightarrow \infty} \alpha \text{dist}_{S_D}(D_k^0) + \beta \|\Delta V_k^0\| = 0, \quad (34)$$

and so  $\text{dist}_{S_D}(D_k^0) \rightarrow 0$  and  $\Delta V_k^0 \rightarrow 0$  for  $k \rightarrow \infty$ , which means that  $S_D$  is attractive for the closed loop, with a domain of attraction given by  $\mathcal{C}_N(\mathcal{D}_s)$ .

#### B. $\epsilon - \delta$ Stability of $S_D$

To properly prove the stability in the sense of Lyapunov ( $\epsilon - \delta$  stability), it is sufficient to find a Lyapunov function. The main property of such a function is that it must be a decreasing function along the state trajectories. Furthermore, it must be bounded from above and below by  $\mathcal{K}_\infty$  functions. The Lyapunov function candidate is (as usual in MPC) the optimal cost  $J_N^0(D)$ . Equation (33) shows that  $J_N^0(D)$  is a decreasing function along the state trajectories. Then, by making some well-known additional conditions (continuity of the system and the cost function, compactness of the constraint sets, and boundness for the stage cost), it is possible to ensure that  $J_N^0(D)$  is in fact a Lyapunov function (see [28], for details).

Finally, merging the attractivity and the  $\epsilon - \delta$  stability of  $S_D$ , it follows that  $S_D$  is asymptotically stable for the aforementioned closed-loop, with a domain of attraction given by  $\mathcal{C}_N(\mathcal{D}_s)$ . ■

*Remark 2:* The present section has established the stability of the set  $S_D$  by means of the control of the discrete-time system (13). However, the property of the targeted set  $S_D$  ensures that the relative trajectories between control instants remains periodic in the hovering zone once reached.

## V. SIMULATION RESULTS

In order to assess the performance of the proposed controller, four hovering scenarios extracted from [20] are simulated. They are described by the spacecraft parameters, the thrusters limits, the hovering zone and the initial states, and are given in Table I. The simulations are executed using a non-linear simulator of the Gauss equations for both spacecraft separately before the relative motion is recovered from the inertial motions [29]. Note that non-Keplerian forces such as the J2 effect and atmospheric drag are considered for both target and chaser spacecraft. The computations are done in Matlab 2015b using Yalmip's [30] together with MOSEK [31] solver.

The tuning parameters of the IzMPC controller are  $\alpha = 1$ ,  $\beta = 1$  and  $\gamma = 1000$  (this latter value was chosen to account for Property 1). The control horizon will be  $N = 3$  and  $N = 10$ , depending on the simulation. On Figure 2, the controlled relative trajectories are depicted, for  $N = 3$  and for different values of  $\Delta \nu$  (the constant distance between two successive anomalies  $\nu$ ). Every simulations shows that the chaser spacecraft is steered to the hovering box using different paths. To asses the performance of each one, three main indexes will be used:

- (i) the normalized distance to  $S_D$ ,

$$\eta(k) = \frac{\|D_k - D_k^*\|_2}{\|D_0 - D_0^*\|_2};$$

- (ii) the normalized value of  $d_0$ ,

$$\hat{d}_0(\nu) = \frac{d_0(\nu)}{d_0(\nu_0)};$$

- (iii) the normalized value of the cost  $J_N$ ,

$$\hat{J}_k = \frac{J_N(D_k)}{J_N(D_0)};$$

$a = 8750$ km, $e=0.2$ , $\nu_0=0$ , Saturation: $\Delta V=0.5$ m/s Hovering box: $[x, \bar{x}, y, \bar{y}, z, \bar{z}]=[50, 150, -25, 25, -25, 25]$ m Leader mass : 462949 kg, drag surface : 1703 $m^2$ , drag coeff. : 3, Deputy mass : 2000 kg, drag surface : 50 $m^2$ , drag coeff. : 2.274, $X_{01} = [400 \ 300 \ -40 \ 0 \ 0 \ 0]^T$ [m,m/s], $X_{02} = [-800 \ 600 \ 200 \ 0 \ 0 \ 0]^T$ [m,m/s], $X_{03} = [-1500 \ 1300 \ 150 \ 0 \ 0 \ 0]^T$ [m,m/s], $X_{04} = [5000 \ 1300 \ 500 \ 0 \ 0 \ 0]^T$ [m,m/s],z
--

TABLE I: Scenario parameters

(iv) the convergence time  $T_\delta$ , defined as the time at which

$$\eta(\nu) \leq \delta, \quad \forall \nu \geq T_\delta,$$

where  $\delta$  is set to 5%

(v) the fuel consumption,

$$J_{\Delta V} = \int_{i=0}^{T_{sim}} \|\Delta V_i\| \delta(\nu - \nu_i) d\nu,$$

where  $T_{sim}$  is the simulation time, settled in 10 periods for all simulations.

We can observe in the simulations that the higher the frequency of the control is, the faster the chaser converge to the hovering box. However, such a result comes at the price of an higher consumption (see Figure 3). In addition, the periodicity of the trajectory is ensured by controlling  $d_0$  to 0 despite the non linearities. Figure 4 shows a monotonic decrease the cost objective over the first 3 orbital period. This observation corroborates the attractivity of set  $S_D$  proved in section IV-A.

The scenarios have been also run for different control horizon and different times between controls. The convergence time and consumption criteria have been collected in table Table II. The previously observed trend is confirmed as the consumption increases with the control frequency. One can observe, also, that for every scenario the consumption decreases as the control horizon grows.

[20] proposes several hybrid controllers that stabilize a given relative orbit (selected for satisfying the the hovering box limits). By comparison with the results from [20], the convergence is faster and consume less fuel in most of case (especially for  $\Delta\nu = 120^\circ$ ). These facts are expected since the controller developed in this paper is optimization-based contrary to the hybrid controllers from [20].

Compared to MPC approach from [19], the proposed approach allows faster convergence but at the price of the increase of the consumption in most of cases. This observation may be explained by the fact that the proposed approach combines the decreasing of the magnitude of  $d_0$  with the convergence to  $S_D$  while in [19], the goal  $d_0 = 0$  is first achieved before converging to  $S_D$ .

## VI. CONCLUSION

The main idea of this paper was to work with an appropriated LTV model and exploit its characteristics to formulate a controller that exhibits several benefits in terms of the applicability and the performance. The so-called Deaconu

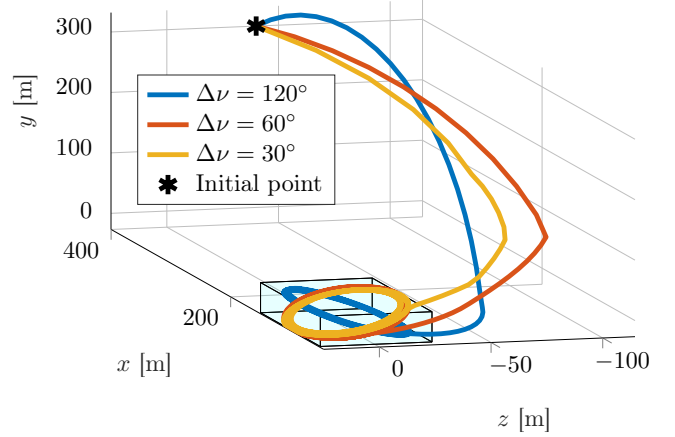


Fig. 2: Relative trajectories from  $X_{01}$  with  $N = 3$  and different  $\Delta\nu$

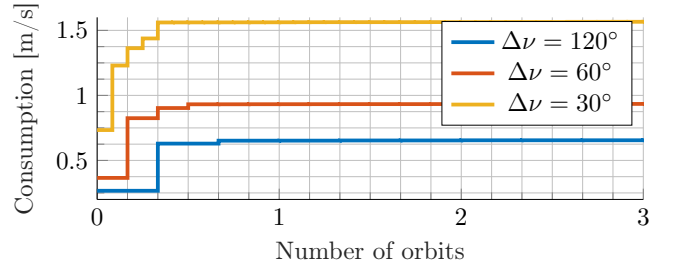


Fig. 3: Consumption for  $N = 3$  over the first 3 periods

parametrization of the relative motion allows to characterize the periodic orbits as the set of equilibrium points. In such context, the predictive controller is shown to be able to steer the system closer and closer to the target set by means of a single feasible control action. The main controller characteristics such as the recursive feasibility and the stability are then deduced from this fact. Furthermore, the controller has a significantly enlarged domain of attraction (given by  $\mathcal{C}_N(\mathcal{D}_s)$ , instead of  $\mathcal{C}_N(S_D)$ , which is the usual case) without using artificial variables (as it is done in the so called MPC for tracking [32]). Simulation results show that the proposed controller exhibits good performances by comparison to other MPC and Hybrid control strategies. Future works include a further study and characterization of the domain of attraction but also robust analysis with respect to control mis-execution errors.

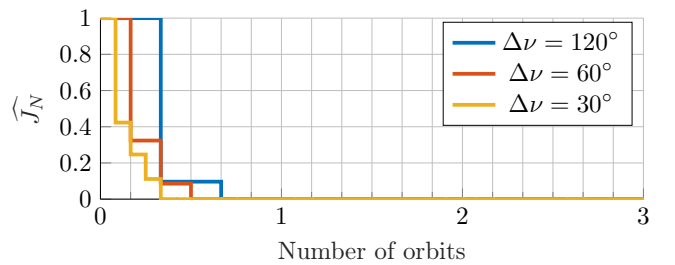


Fig. 4: Normalized cost for  $N = 3$  over the first 3 periods

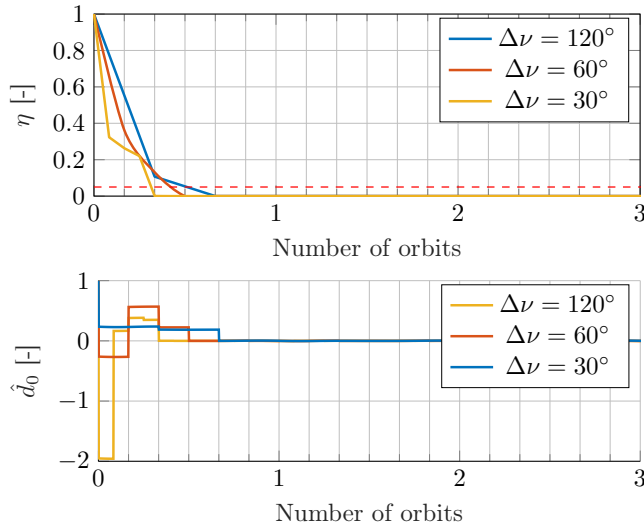


Fig. 5: Convergence criteria for  $N = 3$ : normalized distance to  $S_D$  and to normalized  $d_0$

		$\Delta\nu$	30°	60°	120°
$X_{01}$	$N = 3$	$t_{5\%}$ [orbit]	0.30	0.41	0.50
		cons. [m/s]	1.58	0.94	0.67
$N = 10$	$t_{5\%}$ [orbit]	0.40	0.46	0.50	
	cons. [m/s]	1.54	0.86	0.66	
$X_{02}$	$N = 3$	$t_{5\%}$ [orbit]	0.40	0.44	0.63
		cons. [m/s]	4.26	2.48	1.36
$N = 10$	$t_{5\%}$ [orbit]	0.41	0.49	0.66	
	cons. [m/s]	3.22	2.10	1.29	
$X_{03}$	$N = 3$	$t_{5\%}$ [orbit]	0.48	0.66	1.38
		cons. [m/s]	6.22	3.97	2.69
$N = 10$	$t_{5\%}$ [orbit]	0.49	1.13	2.91	
	cons. [m/s]	4.7	2.69	2.46	
$X_{04}$	$N = 3$	$t_{5\%}$ [orbit]	0.73	0.97	1.38
		cons. [m/s]	8.74	7.25	6.35
$N = 10$	$t_{5\%}$ [orbit]	0.74	2.10	3.40	
	cons. [m/s]	10.64	7.32	4.55	

TABLE II: Convergence time and consumption over 10 periods

#### APPENDIX

Next a property of the rendezvous hovering problem described using the Deaconu parametrization. This property is useful for the closed-loop stability proof is presented. It basically states that a state in  $\mathcal{D}_s$  can be steered in one step to another state in  $\mathcal{D}_s$  such that the distance to  $S_D$  is reduced.

*Property 1:* Let consider fixed scalars  $\alpha \geq 0$  and  $\beta \geq 0$ , and a compact and convex set  $S_D$ , with a sufficiently smooth boundary  $\partial S_D$ . For each  $D_k \in \mathcal{D}_s$ , there exists a feasible  $\widehat{\Delta V}$  (i.e.,  $\|\widehat{\Delta V}\|_\infty \leq \overline{\Delta V}$ ) and a (large enough) scalar  $\gamma \geq 0$  such that:

- (i)  $D_{k+1} \in \mathcal{D}_s$  and
- (ii)  $\gamma \text{dist}_{S_D}(D_{k+1}) + (\alpha \text{dist}_{S_D}(D_k) + \beta \|\Delta V_k\|) \leq \gamma \text{dist}_{S_D}(D_k)$ , where  $D_{k+1} = \Phi_k D_k + B_k \widehat{\Delta V}$ .

where  $D_{k+1} = \Phi_k D_k + B_k \widehat{\Delta V}$ .

Only a sketch of the proof will be given, for the sake of brevity.

*Sketch of the Proof 1:* For a given state  $D_k \in \mathcal{D}_s$ , and an input  $\widehat{\Delta V}$ , the free response of the system, after the jump

(discontinuity) produced by the input  $\widehat{\Delta V}$  is given by

$$D_{k+1} = \Phi_k \left[ \overbrace{D_k + B_D(\nu_k) \widehat{\Delta V}}^{D_k^+} \right],$$

which represents the free response of the system, after the jump (discontinuity) produced by the input  $\widehat{\Delta V}$ . If only the first row of the later matrix equation is considered, the evolution of state  $d_0$  is given by:

$$d_0^+(\nu_k) = d_0(\nu_k) + B_{d_0}(\nu_k) \widehat{\Delta V},$$

where  $B_{d_0}(\nu_k) \triangleq \frac{1}{k^2(e^2-1)} [1 + e \cos \nu_k \quad 0 \quad -e \sin \nu_k]$ . Given that  $D_k \in \mathcal{D}_s$ , (i.e.  $d_0(\nu_k) = 0$ ), the condition  $D_k^+ \in \mathcal{D}_s$  and consequently  $D_{k+1} \in \mathcal{D}_s$  (i.e.  $d_0(\nu_{k+1}) = 0$ ) is obtained if and only if the  $\widehat{\Delta V}$  is chosen such that

$$\frac{1}{k^2(e^2-1)} [1 + e \cos \nu_k \quad 0 \quad -e \sin \nu_k] \widehat{\Delta V} = 0. \quad (35)$$

The latter condition is satisfied with the control input defined by  $\widehat{\Delta V} = \lambda B_{d_0}^\perp(\nu_k)$ , where  $\lambda$  is a scalar to be determined and  $B_{d_0}^\perp(\nu_k) \in \mathbb{R}^3$  is a basis of the kernel space of  $B_{d_0}(\nu_k)$ ,

$$B_{d_0}^\perp(\nu_k) = [e \sin(\nu_k) \quad 0 \quad 1 + e \cos(\nu_k)]^T.$$

This way, the proposed input  $\widehat{\Delta V}$  keeps  $d_0(\nu_{k+1}) = 0$ , but also provides the necessary degrees of freedom (given by  $\lambda$ ) to both, be feasible ( $\|\widehat{\Delta V}\|_\infty \leq \overline{\Delta V}$ ) and steer the whole state  $D(\nu_{k+1})$  closer to  $S_D$ .

From a geometrical point of view, given that  $S_D$  is convex and its boundary sufficiently smooth, there exists an open cone at  $D_k$ , given by the orthogonal direction to  $(D_k - D^*)$ , where  $D^*$  is the closest state to  $D_k$  inside  $S_D$ , containing all the directions such that (it is possible to get)  $\text{dist}_{S_D}(D_{k+1}) < \text{dist}_{S_D}(D_k)$  (see Figure 6). Given that  $\lambda$  can be either positive or negative, the only possible situation in which  $D_{k+1} = D_k + B_D(\nu_k) B_{d_0}^\perp(\nu_k) \lambda$  cannot be placed in the cone is when the difference vector  $(D_{k+1} - D_k)$  is orthogonal to  $(D_k - D^*)$ .

In such a case, it is possible to select the feasible input  $\widehat{\Delta V} = 0$ , which trivially leads to  $\text{dist}_{S_D}(D_{k+1}) = \text{dist}_{S_D}(D_k)$ . Then, in the next step, and given that

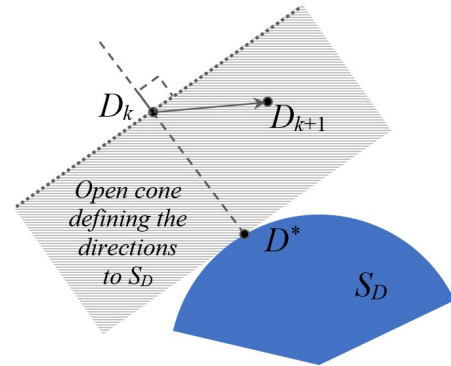


Fig. 6: Schematic plot of the cone of directions minimizing the distance to  $S_D$ .



$B_D(\cdot)B_{d_0}^+(\cdot)$  is a periodic function,  $B_D(\nu_{k+1})B_{d_0}^+(\nu_{k+1})$  will be necessarily different from  $B_D(\nu_k)B_{d_0}^+(\nu_k)$ , thus giving a different direction to the difference vector  $(D_{k+1}-D_k)$ . In such a case, it always exists a scalar  $\lambda$ , small enough, to get  $\text{dist}_{S_D}(D_{k+1}) < \text{dist}_{S_D}(D_k)$ . This means that - even when the first step does not (strictly) reduce the distance to  $D^*$  - it will take at most two steps to do that, which does not affect the convergence result.

This way, in general, it is  $\|D_{k+1}-D^*\| < \|D_k-D^*\|$  for a state  $D^* \in S_D$  or, what is the same,  $\|D_{k+1}-D^*\| < \|D_k-D^*\|$ . Finally, given that  $\overline{\Delta V}$  is bounded by  $\overline{\Delta V}$ , it there exists a scalar  $\gamma$ , large enough, such that:  $\gamma(\text{dist}_{S_D}(D_{k+1})-\text{dist}_{S_D}(D_k)) \leq -(\alpha \text{dist}_{S_D}(D_k) + \beta\|\overline{\Delta V}_k\|)$ .

## REFERENCES

- [1] Reed B. B., Smith R. C., Naasz B. J., Pellegrino J. F., and Bacon C. E. The restore-1 servicing mission. In *AIAA SPACE 2016*. American Institute of Aeronautics and Astronautics, sep 2016.
- [2] Tao Yang. *Impulsive Control Theory*. LNCIS. Springer-Verlag Berlin Heidelberg, 1 edition, September 2001.
- [3] Hartley E.N. A tutorial on model predictive control for spacecraft rendezvous. In *2015 European Control Conference (ECC)*. IEEE, jul 2015.
- [4] Capello E., Dabbene F., Guglieri G., and Punta E. “flyable” guidance and control algorithms for orbital rendezvous maneuver. *SICE Journal of Control, Measurement, and System Integration*, 11(1):14–24, 2018.
- [5] L. S. Breger and J. P. How. Safe trajectories for autonomous rendezvous of spacecraft. *Journal of Guidance, Control, and Dynamics*, 31(5):1478–1489, 2008.
- [6] A. Richards, T. Schouwenaars, J. P. How, and E. Feron. Spacecraft trajectory planning with avoidance constraints using mixed-integer linear programming. *Journal of Guidance, Control, and Dynamics*, 25(4):755–764, July 2002.
- [7] J. B. Mueller and R. Larsson. Collision avoidance maneuver planning with robust optimization. In *International ESA Conference on Guidance, Navigation and Control Systems, Tralee, County Kerry, Ireland*, 2008.
- [8] D. J. Irvin, R. G. Cobb, and T. A. Lovell. A general methodology for minimum-fuel hovering satellite formation. *Advances in the Astronautical Sciences*, 129:329–349, 2007.
- [9] H. Park, C. Zagaris, J. Virgili Llop, R. Zappulla, I. Kolmanovsky, and M. Romano. Analysis and experimentation of model predictive control for spacecraft rendezvous and proximity operations with multiple obstacle avoidance. In *AIAA/AAS Astrodynamics Specialist Conference*. American Institute of Aeronautics and Astronautics, sep 2016.
- [10] R. C. Shekhar and J. M. Maciejowski. Optimal constraint tightening policies for robust variable horizon model predictive control. In *51st IEEE Conference on Decision and Control (CDC)*, pages 5170–5175, December 2012.
- [11] G. Deaconu, C. Louembet, and A. Th eron. Minimizing the effects of navigation uncertainties on the spacecraft rendezvous precision. *Journal of Guidance, Control, and Dynamics*, 37(2):695–700, February 2014.
- [12] F. Camps, P. R. Arantez Gilz, M. Joldes, and Ch. Louembet. Embedding a SDP-based control algorithm for the orbital rendezvous hovering phases. In *2018 25th Saint Petersburg International Conference on Integrated Navigation Systems (ICINS)*. IEEE, may 2018.
- [13] Edward N. Hartley and Jan M. Maciejowski. Field programmable gate array based predictive control system for spacecraft rendezvous in elliptical orbits. *Optimal Control Applications and Methods*, 36(5):585–607, mar 2014.
- [14] Alejandro H Gonz alez, Pablo S Rivadeneira, Antonio Ferramosca, Nicolas Magdelaine, and Claude H Moog. Impulsive zone mpc for type i diabetic patients based on a long-term model. *IFAC-PapersOnLine*, 50(1):14729–14734, 2017.
- [15] P. S. Rivadeneira, A. Ferramosca, and A. H. Gonz alez. Control strategies for nonzero set-point regulation of linear impulsive systems. *IEEE Transactions on Automatic Control*, 63(9):2994–3001, 2018.
- [16] Pantelis Sotasakis, Panagiotis Patrinos, Haralambos Sarimveis, and Alberto Bemporad. Model predictive control for linear impulsive systems. *IEEE Transactions on Automatic Control*, 60(8):2277–2282, 2015.
- [17] Georgia Deaconu, Christophe Louembet, and Alain Th eron. Designing continuously constrained spacecraft relative trajectories for proximity operations. *Journal of Guidance, Control, and Dynamics*, 38(7):1208–1217, 2015.
- [18] P. R. Arantes Gilz, M. Joldes, C. Louembet, and F. Camps. Model predictive control for rendezvous hovering phases based on a novel description of constrained trajectories. In *IFAC World Congress*, pages pp. 7490–7495, Toulouse, France, July 2017.
- [19] Paulo Ricardo Arantes Gilz, Mioara Maria Joldes, Christophe Louembet, and Fr ed eric Camps. Stable Model Predictive Strategy for Rendezvous Hovering Phases Allowing for Control Saturation. submitted to *AIAA Journal of Guidance, Control, and Dynamics*, 2018.
- [20] M. Brentari, S. Urbina, D. Arzelier, C. Louembet, and L. Zaccarian. A hybrid control framework for impulsive control of satellite rendezvous. *IEEE Transactions on Control Systems Technology*, (99):1–15, 2018.
- [21] Wigbert Fehse. *Automated rendezvous and docking of spacecraft*, volume 16. Cambridge university press, 2003.
- [22] J. Tschauner. Elliptic orbit rendezvous. *AIAA Journal*, 5(6):1110–1113, 1967.
- [23] K. Yamanaka and F. Ankersen. New state transition matrix for relative motion on an arbitrary elliptical orbit. *Journal of guidance, control, and dynamics*, 25(1):60–66, 2002.
- [24] G. Gaias and S. D’Amico. Impulsive maneuvers for formation reconfiguration using relative orbital elements. *Journal of Guidance, Control, and Dynamics*, 38(6):1036–1049, jun 2015.
- [25] D. J. Irvin, R. G Cobb, and T. A. Lovell. An investigation of teardrop relative orbits for circular and elliptical chief satellites. *Advances in the Astronautical Sciences*, 134:121–140, 2009.
- [26] Pini Gurfil. Relative motion between elliptic orbits: generalized boundedness conditions and optimal formationkeeping. *Journal of Guidance, Control, and Dynamics*, 28(4):761–767, 2005.
- [27] Y. Nesterov. Squared functional systems and optimization problems. In J.B.G. Frenk et al., editor, *High performance optimization*. Kluwer Academic Publishers, 2000.
- [28] J. B. Rawlings, D. Q. Mayne, and M. Diehl. *Model Predictive Control: Theory, Computation, and Design*. Nob Hill Publishing, 2017.
- [29] P. R. Arantes Gilz. A Matlab /Simulink  non-linear simulator for orbital spacecraft rendezvous applications., December 2016.
- [30] Johan L fberg. Yalmip: A toolbox for modeling and optimization in matlab. In *Proceedings of the CACSD Conference*, volume 3. Taipei, Taiwan, 2004.
- [31] Erling D Andersen and Knud D Andersen. The mosek interior point optimizer for linear programming: an implementation of the homogeneous algorithm. In *High performance optimization*, pages 197–232. Springer, 2000.
- [32] D. Limon, I. Alvarado, T. Alamo, and E. F. Camacho. MPC for tracking of piece-wise constant references for constrained linear systems. *Automatica*, 44(9):2382–2387, 2008.